Can parameterizations reproduce the gravity waves momentum fluxes and drag simulated by a global high-resolution model?

I. Toghraei[1], F. Lott[1], L. Köhler[2], C. C. Stephan[3], M. J. Alexander[4]

[1]Laboratoire de Météorologie Dynamique, Institut Pierre-Simon Laplace, PSL Research Institute, Paris, France.
[2]Alfred Wegener Institute, Bremerhaven, Germany.
[3]Leibniz Institute of Atmospheric Physics, University of Rostock, Kühlungsborn, Germany.
[4]NorthWest Research Associates, Boulder Office, Boulder, CO, USA

keypoints

- In the lower stratosphere, parameterizations simulate well the regions where gravity waves are large in a high-resolution global model.
- An attenuation of the resolved gravity waves aloft the subtropical jets is described by the parameterization but is underestimated.
- The parameterizations give good estimates of the mountain waves but underestimate the convective waves and overestimate the frontal waves.

Corresponding author: Francois Lott, `francois.lott@lmd.ipsl.fr`

Abstract

We compare the gravity wave (GW) parameterizations used in the IPSLCM6 climate model with the GWs resolved in the ICON global model with 5 km horizontal resolution. The parameterizations are run offline using ICON fields coarse-grained to a 100 km grid and compared to the GWs with smaller scales that are resolved in ICON. Overall, the drags are comparable, the momentum fluxes align well, and each GW parameterization (fronts, convection, and mountains) plays a role at geographical locations consistent with ICON. Among the differences, we find that in ICON, GWs are substantially attenuated aloft the subtropical jets; this is underestimated by the parameterizations. It could be corrected by tuning the characteristic phase speeds or the breaking criteria in the parameterizations. It also seems that ICON underestimates frontal waves in the mid-latitudes, that the parameterizations underestimate the convective waves in the tropics, and that the mountain waves are more alike.

Plain Language Summary

To simulate the middle atmosphere, climate models use parameterizations of small-scale gravity waves that are generated in the troposphere and break in the middle atmosphere. The direct in situ observations of these waves are sparse and non-global, while remotely-sensed satellite observations are more global but have quite coarse resolutions. To compensate for these deficiencies, the recent high-resolution global simulations of the earth atmosphere are promising because they explicitly solve a good fraction of the gravity wave spectra and their dissipation. Here we show that these simulations can help to validate relationships of parameterized gravity waves to their sources and to adjust their characteristic phase speed. Such comparisons can also establish whether high-resolution simulations resolve enough GW momentum flux to simulate the observed middle atmosphere climate.

1 Introduction

Gravity waves (GWs) are generated by various sources, such as flow over mountains (Lilly & Kennedy, 1973), convection (Fovell et al., 1992), and imbalances in jets and fronts (Plougonven & Zhang, 2014). As GWs propagate vertically, they carry horizontal momentum and affect the large-scale circulation when they break (Dunkerton, 1997; Alexander & Rosenlof, 2003; Fritts & Alexander, 2003; McLandress & Shepherd, 2009). Since the horizontal scale of the GWs can be much shorter than the 1^o to 2^o horizontal resolution of climate models, they need to be parameterized (Alexander et al., 2010). State-of-the-art GW parameterization schemes use quite a distinct treatment for orographic GWs compared to non-orographic GWs.

In the orographic GW schemes, quite local and detailed information about the source is explicitly taken into account. Such orographic GW parameterizations have been used for almost 40 years and have proven to be successful in reducing biases in the troposphere (Palmer et al., 1986; Lott, 1999; Scinocca & McFarlane, 2000). They have been validated by dedicated in situ observations during field campaigns (Lott & Miller, 1997; Smith & Kruse, 2018) and high-resolution limited area model simulations, i.e., validations that remain very local in space and time. In the non-orographic GW schemes, the numerical and theoretical complexities of treating a large ensemble of waves have led to the development of global spectral schemes (Hines, 1997; Warner & McIntyre, 1999) or to stochastic methods (Lott et al., 2012). Among these schemes, some include sources from convection (Beres et al., 2005; Song & Chun, 2005; Richter et al., 2010; Lott & Guez, 2013a) and fronts in mid-latitudes (Charron & Manzini, 2002; Richter et al., 2010; De la Cámara & Lott, 2015). These non-orographic GW parameterizations reduce biases in the middle atmosphere (Scinocca, 2003; Song & Chun, 2005; Beres et al., 2005; Orr et al., 2010;

Lott & Guez, 2013a; De la Cámara & Lott, 2015; Bushell et al., 2015; Anstey et al., 2016; Serva et al., 2018), which is an indirect proof of their realism.

With the most recent global satellite observations, it becomes possible to gain a global view of the GW fields. However, these only detect large horizontal- and/or vertical-scale GWs and mostly measure temperature fluctuations (Geller et al., 2013a): the momentum fluxes are computed indirectly using polarization relations (Alexander et al., 2010; Ern et al., 2014). In order to observe the shorter horizontal scales and to have more direct access to the momentum fluxes, in situ observations are provided by constant-level long-duration balloons like those made in the Antarctic region during Strateole, Vorcore (Hertzog, 2007) and Concordiasi (Rabier et al., 2010), or in the deep tropics during Pre-Concordiasi (Jewtoukoff et al., 2013) and Strateole 2 (Haase et al., 2018). These observations have helped improve parameterizations of GWs (Alexander et al., 2021; Lott et al., 2023) but remain regional, and limited to the lower stratosphere (Geller et al., 2013b; Achatz et al., 2024).

Global high-resolution models offer a promising avenue to supplement these limitations. First, in these models, the GW fields start to look rather realistic compared to satellite observations (Kruse et al., 2022; Gupta, Reichert, et al., 2024), with the limit that the GW dynamics in these models remains dependent on the model formulation (Wedi et al., 2020; Stephan et al., 2019). Secondly, these models start to reveal the resolution at which GWs no longer need to be parameterized, which is around 1 km or even finer (Polichtchouk et al., 2023; Gupta, Reichert, et al., 2024). If true, it means that parameterizations will remain necessary in most climate models for the foreseeable future (Achatz et al., 2024). Third, high-resolution models provide valuable recommendations for improving GW parameterizations. For example, Kruse et al. (2022) and Gupta, Reichert, et al. (2024) highlight the necessity of including lateral propagation, and Polichtchouk et al. (2023) highlight the need to reconsider the partitioning between the different sources. For instance, it is essential to achieve the correct balance between orographic, frontal and convective GWs to simulate well the Northern Hemisphere (NH), the Southern Hemisphere (SH), and the quasi-biennial oscillation in the tropics (de la Cámara et al., 2016).

Based on the success of the GW parameterization schemes to simulate a realistic climate, the purpose of this paper is to evaluate momentum fluxes parameterized in climate models by comparing them to those explicitly resolved in a recent state-of-the-art high-resolution model. This comparison is an essential step in bridging the gap between observations, models, and parameterizations and has practical applications. One is to determine if high-resolution models produce the right amount of waves, and another is to assess if the GW dynamics at work in parameterizations are consistent with the GW dynamics in high-resolution models. To reach these goals, we first use a simulation performed with the ICOsahedral Nonhydrostatic Weather and Climate Model (ICON) at a resolution around 5 km. The fields from this model are "coarse-grained" at horizontal scales near 1^o to mimic the grid scale of a climate model. Then, subgrid-scale fluxes in the full-resolution model are defined as those with scales less than the coarse-grained resolution. We second run the GW parameterizations that are operational in the Institut Pierre-Simon Laplace Coupled Model version for CMIP6 (IPSLCM6, Boucher et al. (2020)) in offline mode using the ICON coarse-grained fields of winds, temperature, and precipitation.

The plan of the paper is as follows: Data and methods are discussed in section §2. In section §3, the "subgrid-scale" GWs drag and fluxes resolved by ICON are compared to the parameterized GWs drag and fluxes across different sectors and altitudes. Section §4 discusses how such a comparison can help improve parameterizations of GWs and/or help estimate whether a high-resolution model produces the right amount of GWs.

2 Data and methods

2.1 Resolved momentum flux

To calculate momentum fluxes due to GWs with horizontal scales smaller than climate models' grid scales, we take 3-hourly instantaneous output from a 5 year ICON run with atmosphere-ocean coupling performed within cycle 3 of the nextGEMS project (Koldunov et al., 2023). We choose ICON because at the resolution of climate models it reasonably simulates the middle atmosphere (Borchert et al., 2019). At the resolution of around 5 km used here, and without deep convection and GW parameterizations, it simulates precipitation realistically (Stevens et al., 2019), it is capable of simulating GWs explicitly (Hohenegger et al., 2023), and its GW fields show similarities when compared to balloon and satellite observations (Köhler et al., 2023; Stephan et al., 2019). These comparisons were carried out for the tropics, where the 5 km resolution is sufficient for an explicit simulation of realistic deep convection (Stevens et al., 2019). The run was initialized from ERA5 on January 20, 2020 and we analyze 3 weeks of data between March 20 and April 10, 2020. Selecting dates near equinox was motivated by the desire to have comparable dynamical filtering conditions for GWs between the two hemispheres in the low stratosphere (e.g., mid-latitude stratospheric jets with positive zonal mean zonal winds in both hemispheres). The horizontal resolution of the icosahedral grid is R2B9 ($\sim$5 km), but the outputs are written on a Hierarchical Equal Area isoLatitude Pixelisation (Healpix) grid with resolution $N_{\text{side}} = 1024$, corresponding to ~ 6.3 km. In the vertical, the model has 90 unequally spaced levels up to $z = 75$ km. In the following, we only consider data up to the top of the stratosphere, $z = 50$ km, below the sponge layer.

To extract GWs, we apply to the horizontal wind field a Helmholtz decomposition between a divergent and a rotational part (Lindborg, 2015), and assume that only the divergent part is associated with GWs (Stephan et al., 2022; Gupta, Sheshadri, & Anantharaj, 2024). We use it to compute cross products, such as uw, with u and w being the zonal and vertical winds, respectively. We then average the original wind fields and cross products to a coarser Healpix grid with a resolution of $N_{\text{side}} = 64$, corresponding to $\sim$100 km. This mapping allows the calculation of the momentum flux,

$$F^z = \rho\,[u'w'] + \rho f \frac{[v'\theta']}{[\theta]_z}, \tag{1}$$

where [ ] is the average over the $N_{\text{side}} = 64$ Healpix coarse-grained grid boxes and $u^{'} = u - [u]$. In addition, ρ is the density, θ is the potential temperature, v is the meridional velocity and f is the Coriolis parameter. In (1), we found that the contribution of the thermal flux $[v'\theta']$ to F^z was always negligible compared to that of $[u'w']$. To quantify the contribution of F^z to the general circulation, we also evaluate its zonal mean (indicated by overlines) and refer to

$$\overline{F}^z = a\cos\phi\left(-\overline{\rho\,[u'w']} + \overline{\rho f \frac{[v'\theta']}{[\theta]_z}}\right), \tag{2}$$

as the contribution of the subgrid-scale waves to the vertical component of the EP flux, with a being Earth's radius and ϕ latitude. For completeness, note that when using ICON data, we always include the meridional component of the Eliassen-Palm flux,

$$\overline{F}^\phi = -a\cos\phi\,\overline{\rho\,[u'v']}, \tag{3}$$

to calculate the zonal mean GW drag, i.e.

$$\frac{1}{\rho a\cos\phi}\left(\frac{\partial\cos\phi\,\overline{F}^\phi}{\partial\phi} + \frac{\partial\overline{F}^z}{\partial z}\right). \tag{4}$$

Note that we found the contribution of $\overline{F}^\phi$ to be small, leaving $\overline{u'w'}$ making the largest contribution to the drag and momentum fluxes. Note also that Procházková et al. (2023)

and Sun et al. (2023) found that $\overline{u'w'}$ is not much sensitive to the method for extracting GWs from high-resolution model data.

2.2 Parameterized momentum flux

The subgrid-scale orography parameterization we use is described in Lott and Miller (1997), the subgrid scale fields being calculated on the IPSLCM6 grid. The non-orographic GW schemes, which include as sources convection and fronts, are described in Lott and Guez (2013b) and De la Cámara and Lott (2015), respectively. None of these schemes include lateral propagation or rotation; they assume $F^y = 0$ and parameterize F^z neglecting the thermal flux. Note that we performed no tuning and kept the setup of IPSLCM6 for a 143×142 lat-lon grid. The parameterizations are then run offline from March 20 to April 10, 2020, using the coarse-grained three-dimensional fields of ICON with calculations performed on the coarse-grained grid. Note that Lott et al. (2023) discuss to what extent such an offline approach gives useful insight into what occurs online.

3 Results

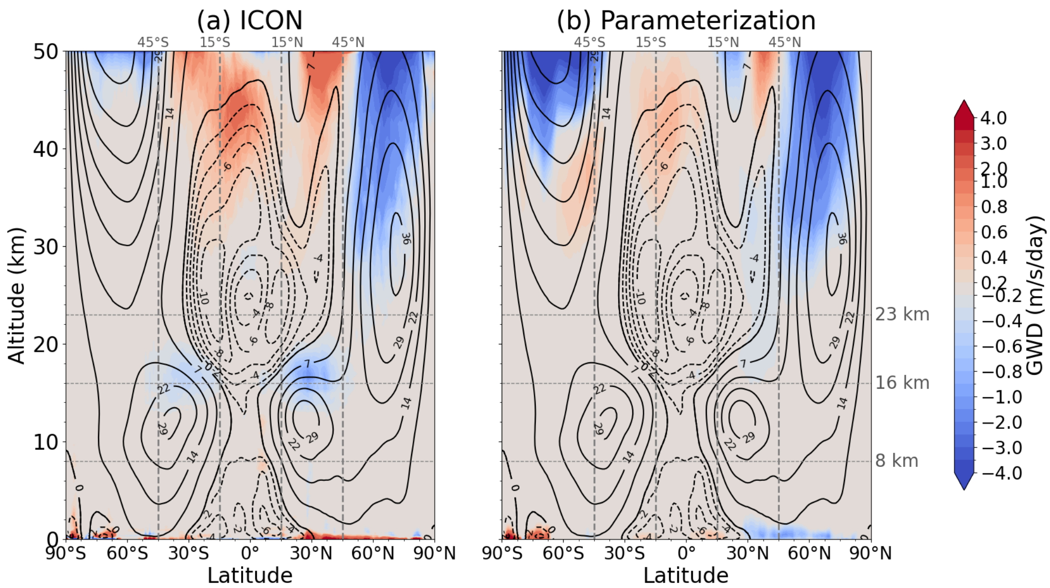

Figure 1. Zonal mean 21-day mean of the resolved (a) and parameterized (b) GW drag. Solid and dashed contour lines represent eastward and westward zonal mean 21-day mean zonal wind, respectively. The gray lines indicate the three altitudes $z = 8$, 16, 23 km at which we analyse the momentum fluxes and the latitudes $\phi = \pm 15^o$, $\phi = \pm 45^o$, we use to dynamically separate the tropics from the subtropics, and the subtropics from the mid-latitudes and polar regions.

Fig. 1 compares the GW drag from the resolved and parameterized waves. In the stratosphere, Fig. 1(a) shows that the resolved waves produce negative drag where the winds are positive with negative vertical shears for instance below the stratopause in the NH on the upper flank of the stratospheric jet (30 km$< z <$ 50 km, $\phi > 45^o$), and in the subtropical regions above the tropospheric jets in both hemispheres (13 km$< z <$ 20 km, $15^o < |\phi| < 35^o$). There are also negative drags in the SH stratospheric jet, again in locations of positive zonal wind (below $z \approx 50$ km, $\phi < -45^o$). In the tropical and subtropical upper stratosphere ($z > 30$ km, -$45^o < \phi < 45^o$), the drag is positive, mostly in locations of negative or low wind speeds with positive shear. Interestingly, the parameterizations in Fig. 1(b) reproduce comparable patterns concerning the sign of the drag, at least in the upper stratosphere. Regarding the amplitudes, resolved and parameterized drags in the upper stratosphere compare well above the NH stratospheric jet core, but the parameterizations underestimate the positive drag in the tropics and overestimate the negative drag in the SH stratospheric jet. Another pronounced difference is that above the tropospheric subtropical jet ($z \approx 16$ km, $15^o < |\phi| < 45^o$), the parameterizations strongly underestimate the negative drags.

It is encouraging that the signs of parameterized drags are largely consistent with those due to resolved waves. It implies that the resolved wave dynamics is well captured by parameterizations representing upward-propagating GWs with origins in the troposphere. The parameterizations are formulated such that negative (positive) intrinsic phase speed waves yield negative (positive) momentum fluxes and break more easily in negative (positive) zonal winds. In the following, we refer to this mechanism as "dynamical filtering".

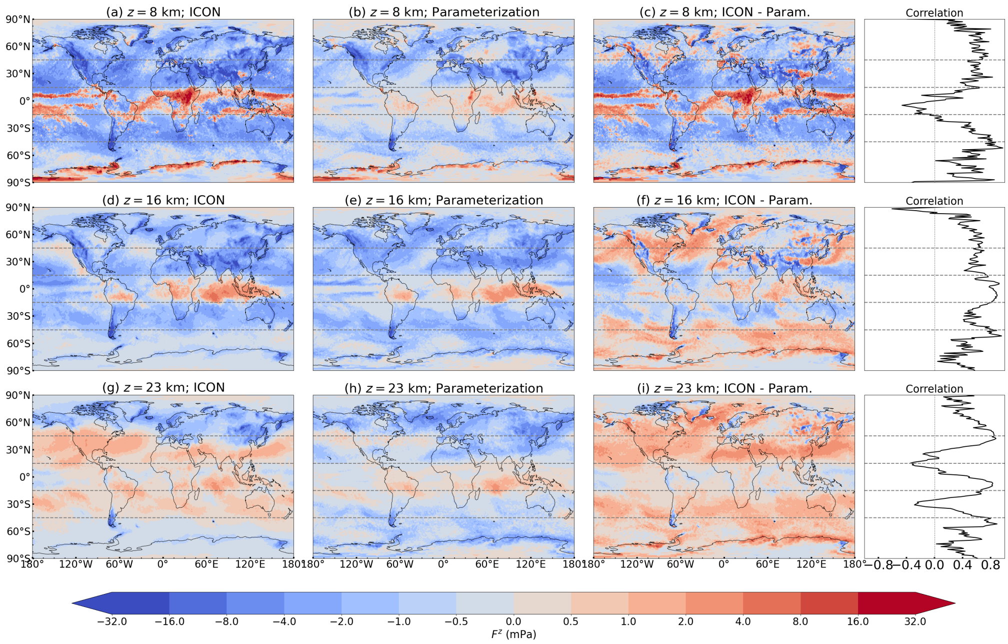

Figure 2. Global distribution of the 21-day mean net zonal momentum fluxes resolved by ICON (left), predicted by the parameterization schemes using ICON meteorological fields (middle), and their difference (right) at (a,b,c) $z = 8$ km, (d,e,f) $z = 16.4$ km, and (g,h,i) $z = 23.9$ km. The correlations between the resolved and parameterized momentum fluxes are presented in the adjacent column.

To test if the resolved and parameterized waves entering the stratosphere originate from the same regions, Fig. 2 shows the geographic distribution of the 21-day averaged momentum fluxes, F^z, at $z = 8$ km (a,b), 16 km (c,d), and 23 km (e,f). We choose these three levels because we found more substantial differences in GWs absorptions in the lower stratosphere than above (see S2). To better evaluate the geographic correspondences, the differences between the resolved and parameterized momentum fluxes are shown in a separate column (Fig. 2(c,f,i)) and the correlations,

$$C(\phi) = \overline{(F_I^z - \overline{F}_I^z)(F_P^z - \overline{F}_P^z)} / \sqrt{\overline{(F_I^z - \overline{F}_I^z)^2}\,\overline{(F_P^z - \overline{F}_P^z)^2}}, \quad (5)$$

are shown as a function of latitude in the adjacent column. In (5), I and P indices denote the resolved and parameterized momentum fluxes, respectively.

In the troposphere at $z = 8$ km in Figs. 2(a,b,c), there are resemblances over the major mountain ranges (Rockies, Andes, and from the Alps to the Tibetan plateau), with the resolved fluxes larger in amplitude than parameterized ones. Over the Rockies, Himalayas, and Tibetan plateau, the difference map in Fig. 2(c) shows changes in sign above the same mountain range. This qualitative difference is certainly due to the fact that the orographic GW scheme does not include lateral propagation (Kruse et al., 2022). In other regions, the patterns agree to a varying extent. Over the oceans and outside the tropics, the resolved and parameterized fluxes have the same sign, the resolved fluxes being substantially larger in the region including the subtropics ($15^o < |\phi| < 45^o$) and quite comparable more poleward ($|\phi| > 45^o$). In the tropics, the differences are much more pronounced. The resolved fluxes are much larger and often of opposite sign compared to the parameterized ones and the correlations are small. In these regions, we recover the results in Wei et al. (2022) or Köhler et al. (2023), who have shown that when there is deep convection, the circulations that are diabatically forced produce momentum fluxes that cannot be explained in terms of upward propagating GWs only.

In the lower stratosphere at $z = 16$ km in Figs. 2(d,e,f), the momentum fluxes show better agreement. They are still quite large and predominantly negative over the mountain ranges in the mid-latitudes and over the oceans away from the tropics. Over the oceans, there is a global shift of the parameterized fluxes toward the polar regions. In the NH, for instance, and over the Atlantic Ocean east of Newfoundland along the storm track, the parameterizations predict intense and negative fluxes whereas the resolved fluxes are small. In the SH, the resolved fluxes have a band of maximum strength around $\phi = -30^o$ (Fig. 2(d)), whereas the parameterized fluxes have a comparable band but centered 10^o poleward (Fig. 2(e)). In the tropics ($|\phi| < 15^o$), the pattern and signs of the fluxes agree well, with positive correlation, although the parameterized fluxes tend to be slightly weaker in amplitude. More specifically, in the eastern Pacific, resolved and parameterized fluxes are strong and negative above the two branches of the Intertropical Convergence Zone (ITCZ), and positive over Brazil, equatorial Africa, the Indian Ocean and the Maritime Continent. It appears that at this altitude and above convective regions, upward propagating GW dynamics are better able to explain momentum fluxes compared to the troposphere.

Whereas the parameterized and resolved fluxes show resemblance at $z = 16$ km, the agreement deteriorates at $z = 23$ km in Figs. 2(g,h,i). The major differences are above the subtropical jets ($15^o < |\phi| < 45^o$), where the resolved fluxes are positive and the parameterized ones negative. In these regions, Fig. 2(g) indicates that the resolved westward waves contributing to the negative fluxes in Fig. 2(d) have been considerably attenuated, whereas the parameterized westward waves continue to dominate. Accordingly, the correlations between the fluxes become small. In the mid-latitudes and polar regions ($|\phi| > 45^o$) over oceans and land, resolved and parameterized fluxes are consistently positive and mostly correlated, but the resolved fluxes are substantially smaller in amplitude.

To shed light on the causes of similarities and differences between the resolved and parameterized fluxes, Fig. 3 shows the contribution of the three GW parameterizations at $z = 16$ km and $z = 23$ km. Over mountainous regions, the orographic GW parameterization is responsible for the major fraction of the negative fluxes. They are substantially attenuated between 16 km and 23 km in the subtropical bands ($15^o < |\phi| < 45^o$) (above the subtropical tropospheric jet) when the zonal wind in the stratosphere becomes small or negative (Fig. 1). For these waves of zero absolute phase speed, this attenuation is caused by "near"-critical level situations and a comparable attenuation is seen in the resolved fluxes in Figs. 2(d) and 2(g).

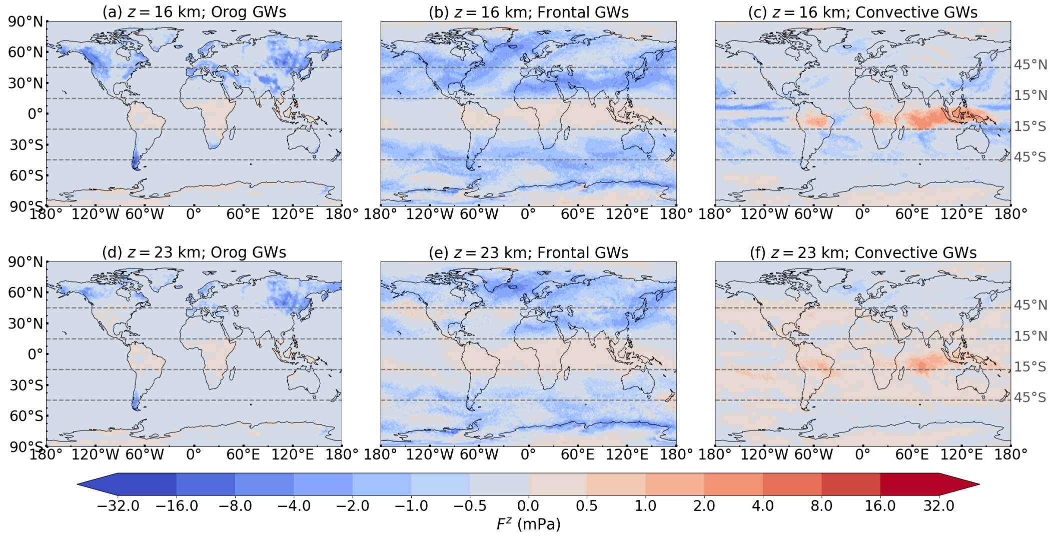

Figure 3. Global distribution of the 21-day mean net zonal parameterized momentum fluxes using ICON meteorological fields: orographic GWs (left), convective GWs (middle), and frontal GWs (right), at $z = 16$ km (first row) and $z = 23$ km (second row).

The frontal GW parameterization (Figs. 3(b) and (e)) produces large negative fluxes from the subtropics to the polar regions ($|\phi| > 15^o$), and is responsible for the excessively large parameterized fluxes at $z = 16$ km in the mid-latitudes (Fig. 2(e)). These westward fluxes are not much attenuated between 16 km and 23 km because in the mid-latitudes and polar regions ($|\phi| > 45^o$), the stratospheric wind is positive in both hemispheres (see Fig. 1). In the subtropics ($15^o < |\phi| < 45^o$), the parameterized frontal waves are not much attenuated between $z = 16$ km and $z = 23$ km, presumably because they have too large phase speeds. The facts that the resolved westward waves (i) have smaller amplitudes in the mid-latitudes and (ii) are more filtered in the subtropics explain most of the positive differences between the resolved and parameterized momentum fluxes in the subtropics and mid-latitudes seen at 23 km in Fig. 2(i) where $|\phi| > 15^o$.

The convective GW parameterization in Figs 3(c) and 3(f) explains most of the parameterized fluxes in the tropics and subtropics, for instance over the Pacific ITCZ, the Maritime Continent and the monsoon regions (Figs. 2(d) and 2(e), respectively). Around the subtropical zones at $\phi = \pm 30^o$, the parameterized convective GW flux is considerably attenuated and changes sign between $z = 16$ km and $z = 23$ km. Such a change of sign is also present in the resolved fluxes around these latitudes (Figs. 2(d) and 2(g)), although much more pronounced. Again and like for orographic waves, this attenuation of the negative intrinsic phase speed waves occurs aloft the tropospheric subtropical jet center, consistent with dynamical filtering. Although the convective GW fluxes have smaller amplitudes than the resolved fluxes, their change in sign between $z = 16$ km and $z = 23$ km and their patterns at $z = 23$ km look qualitatively comparable in the tropics and subtropics (for the resolved waves see Figs. 2(d) and 2(g), and the peak in correlation compared to the subtropics).

Considering net fluxes hides the fact that negative and positive phase speed waves can lead to cancelling momentum fluxes but result in drags of opposite signs at different altitudes. With the approach of identifying momentum fluxes in ICON taken here, it is impossible to separate eastward and westward waves. As supporting information, we therefore propose to assume that the net fluxes of a given sign at a given time are associated with GWs of corresponding intrinsic phase speed sign. The method is not ideal, we can underestimate the fluxes when there are phase speed symmetries, but easy to implement.

Fig. S1 shows that the temporal averages of these sign definite fluxes have amplitudes comparable with the net fluxes in Fig. 2. It also shows that the resolved and parametrized fluxes continue to be comparable. More specifically, away from the tropics ($|\phi| > 15^o$), Figs. S1(a,b,e,f) show that at $z = 16$ km, the westward fluxes strongly dominate the eastward fluxes as expected for mountain waves and also because the tropospheric zonal winds are predominantly positive and favouring westward waves above. Comparing Figs. S1(a) and S1(c) show that the resolved westward waves are strongly absorbed above the subtropical jet ($15^o < |\phi| < 45^o$), and much more than the parameterized ones in S1(b) and S1(d). In the tropics ($|\phi| < 15^o$), there is a strong longitudinal variations with the westward fluxes dominating over the Pacific ITCZ at $z = 16$km (S1(c) and S1(d)), and the eastward fluxes dominating elsewhere (S1(e) and S1(f)). The westward fluxes seem more attenuated than the eastward fluxes between $z = 16$km and $z = 23$km, presumably because the wind shear is predominantly positive in the tropical lower stratosphere (Fig. 1).

For a more quantitative depiction, Fig. S2(a,b,c,d) present their vertical profiles averaged over the four sectors we have used so far to characterize the momentum flux behaviour, i.e. mountainous regions, defined as standard deviation of subgrid-scale orography $\sqrt{[h'^2]} > 100$ m, and non-mountainous regions (land and ocean) in the mid-latitudes ($|\phi| > 45^o$), the subtropics ($15^o < |\phi| < 45^o$), and the tropics ($|\phi| < 15^o$). In all panels, and as expected from the comparisons at the three levels analyzed before ($z = 8, 16, 23$ km), the resolved fluxes (solid lines) are systematically larger than the parameterized ones (dashed lines) in the upper troposphere but decay rapidly with altitude in the lower stratosphere. The $z \simeq 16$ km level is where the fluxes almost intersect. More specifically, the fluxes over the mountain regions are those for which there are the best correspondences, dominated by westward waves, and for the parameterized waves, the contribution of the subgrid-scale orographic waves make the larger contribution. In the mid-latitudes, the parameterized waves dominate in the lower stratosphere and are slightly less attenuated than the resolved ones between $z = 16$ km and $z = 23$ km. In the subtropics between $z = 16$ km and $z = 23$ km, the westward resolved waves are strongly attenuated. In the tropics, the resolved fluxes are greater at all levels. Aloft $z = 23$ km, the decay rates of all the fluxes with altitude become more comparable.

4 Conclusion

This study uses high-resolution simulations of the ICON model to estimate the momentum fluxes due to disturbances with horizontal scales shorter than ≈ 100 km, representative of the grid of a climate model. These momentum fluxes are then predicted by the GW parameterization schemes used in the IPSLCM6 climate model, the input fields for the parameterizations being the ICON fields on an appropriately coarse-grained grid. A key finding is that the momentum fluxes and drag in the stratosphere are quite well predicted in terms of amplitude and geographical distribution. When we split the analysis between sectors and parameterizations, we found that the high-resolution model and the parameterizations show the best agreement over mountainous regions, where the Lott and Miller (1997) parameterization is most relevant. In the mid-latitudes, the parameterizations overestimate the fluxes, which we attributed to the De la Cámara and Lott (2015) parameterization of frontal waves, whereas in the tropics, the parameterizations underestimate the fluxes, which we attribute to the Lott and Guez (2013a) parameterization of convective GWs. The non-orographic parameterizations also underestimate the dynamical filtering of the westward propagating GWs above the subtropical jet.

If we take the high-resolution model as the truth, these discrepancies could be corrected, for instance, by decreasing the tuning parameter that controls the drag amplitude in the frontal scheme and increasing the one that controls the convective GW amplitude. To improve the dynamical filtering aloft the subtropical jet, we could decrease the parameter that controls the intrinsic phase speeds of the non-orographic GWs. Preliminary offline tests show that these changes indeed improve some aspects of the comparison. Improving the statistical distributions is more challenging since in parameterizations the intermittency of the momentum fluxes is in good part related to the way we relate the GWs with their sources (de la Cámara et al., 2014). In the frontal scheme, they are directly related to the square of grid-scale vorticity and in the convective GW schemes to the square of grid-scale precipitation. Reconsidering these relations certainly calls for more advanced analysis, like ENKF parameter estimation of the launch momentum fluxes to better determine what causes large momentum fluxes in the lower stratosphere (Tandeo et al., 2015). In any case, such parameter estimations are limited by the fact that our parameterizations neglect lateral propagation (Voelker et al., 2024). Taking it into account is numerically costly and may require approaches based on machine learning (Matsuoka et al., 2020; Espinosa et al., 2022).

The similarities and differences we find here are certainly model and parameterization dependent. This is a deliberate choice: the parameterization schemes used have not been tuned prior to the comparison, and the middle-atmosphere climatology of the ICON high-resolution simulations we use has not yet been thoroughly validated. Nevertheless, the stratospheric jets shown in Fig. 1 are quite strong compared to climatology, a quite systematic error during all seasons of the run analysed (not shown), suggesting that the resolved GW drag is too small. In the tropics, the QBO rapidly fades away (at the initial time of the run, the zonal winds in the lower tropical stratosphere are much stronger than shown in Fig. 1), which may also indicate improper GWs forcing. However, note that Giorgetta et al. (2022) used a comparable version of ICON and found GWs forcing in the QBO region that are quite reasonable. In this respect, our results can also serve as guidance to judge wave forcing in high-resolution models. After all, the parameterizations have been tuned to reproduce a correct mean climate in the middle atmosphere. For example, we have seen that the frontal waves parameterization predicts larger momentum fluxes than ICON simulates, but it is possible that the resolved waves are underestimated in ICON. Indeed, high-resolution simulations have not yet converged when it comes to GWs in the extratropics (Polichtchouk et al., 2023; Gupta, Reichert, et al., 2024) and should not be considered true. Other parameterizations or numerical implementations may also affect the GW impact (e.g., dissipation). At least for convective waves there is substantial evidence that their amplitude in high-resolution models is very sensitive to model formulation (Stephan et al., 2022). Accordingly, and in all regions, the GW drags predicted by the parameterizations become an important upper bound to validate the high-resolution models. Systematically tuning the GW parameterizations to improve their fit with high-resolution simulations could be a fruitful endeavour to learn about deficits in the parameterizations as well as deficits in resolved dynamics.

Open Research

All data and routines needed to run the parameterizations offline and to compare the results with the coarse-grained ICON fields can be downloaded from Zenodo (Toghraei, 2024).

Acknowledgments

This work was supported by the VESRI Schmidt Future project "Datawave".

References

Achatz, U., Alexander, M., Becker, E., Chun, H.-Y., Dörnbrack, A., Holt, L., . . . others (2024). Atmospheric gravity waves: Processes and parameterization. *Journal of the Atmospheric Sciences*, *81*(2), 237–262.

Alexander, M. J., Geller, M., McLandress, C., Polavarapu, S., Preusse, P., Sassi, F., . . . others (2010). Recent developments in gravity-wave effects in climate models and the global distribution of gravity-wave momentum flux from observations and models. *Quarterly Journal of the Royal Meteorological Society*, *136*(650), 1103–1124.

Alexander, M. J., Liu, C., Bacmeister, J., Bramberger, M., Hertzog, A., & Richter, J. (2021). Observational validation of parameterized gravity waves from tropical convection in the whole atmosphere community climate model. *Journal of Geophysical Research: Atmospheres*, *126*(7), e2020JD033954.

Alexander, M. J., & Rosenlof, K. H. (2003). Gravity-wave forcing in the stratosphere: Observational constraints from the upper atmosphere research satellite and implications for parameterization in global models. *Journal of Geophysical Research: Atmospheres*, *108*(D19).

Anstey, J. A., Scinocca, J. F., & Keller, M. (2016). Simulating the qbo in an atmospheric general circulation model: Sensitivity to resolved and parameterized forcing. *Journal of the Atmospheric Sciences*, *73*(4), 1649 - 1665. doi: https://doi.org/10.1175/JAS-D-15-0099.1

Beres, J. H., Garcia, R. R., Boville, B. A., & Sassi, F. (2005). Implementation of a gravity wave source spectrum parameterization dependent on the properties of convection in the whole atmosphere community climate model (waccm). *Journal of Geophysical Research: Atmospheres*, *110*(D10). doi: https://doi.org/10.1029/2004JD005504

Borchert, S., Zhou, G., Baldauf, M., Schmidt, H., Zängl, G., & Reinert, D. (2019). The upper-atmosphere extension of the icon general circulation model (version: ua-icon-1.0). *Geoscientific Model Development*, *12*(8), 3541–3569. Retrieved from `https://gmd.copernicus.org/articles/12/3541/2019/` doi: 10.5194/gmd-12-3541-2019

Boucher, O., Servonnat, J., Albright, A. L., Aumont, O., Balkanski, Y., Bastrikov, V., . . . Vuichard, N. (2020). Presentation and evaluation of the ipsl-cm6a-lr climate model. *Journal of Advances in Modeling Earth Systems*, *12*(7), e2019MS002010. doi: https://doi.org/10.1029/2019MS002010

Bushell, A. C., Butchart, N., Derbyshire, S. H., Jackson, D. R., Shutts, G. J., Vosper, S. B., & Webster, S. (2015). Parameterized gravity wave momentum fluxes from sources related to convection and large-scale precipitation processes in a global atmosphere model. *Journal of the Atmospheric Sciences*, *72*(11), 4349–4371. doi: https://doi.org/10.1175/JAS-D-15-0022.1

Charron, M., & Manzini, E. (2002). Gravity waves from fronts: Parameterization and middle atmosphere response in a general circulation model. *Journal of the Atmospheric Sciences*, *59*(5), 923 - 941. doi: 10.1175/1520-0469(2002)059⟨0923:GWFFPA⟩2.0.CO;2

De la Cámara, A., & Lott, F. (2015). A parameterization of gravity waves emitted by fronts and jets. *Geophysical Research Letters*, *42*(6), 2071–2078.

de la Cámara, A., Lott, F., & Abalos, M. (2016). Climatology of the middle atmosphere in lmdz: Impact of source-related parameterizations of gravity wave drag. *Journal of Advances in Modeling Earth Systems*, *8*(4), 1507-1525. doi: https://doi.org/10.1002/2016MS000753

de la Cámara, A., Lott, F., & Hertzog, A. (2014). Intermittency in a stochastic parameterization of nonorographic gravity waves. *Journal of Geophysical Research: Atmospheres*, *119*(21), 11,905-11,919. doi: https://doi.org/10.1002/2014JD022002

Dunkerton, T. J. (1997). The role of gravity waves in the quasi-biennial oscillation. *Journal of Geophysical Research: Atmospheres*, *102*(D22), 26053–26076.

Ern, M., Ploeger, F., Preusse, P., Gille, J., Gray, L. J., Kalisch, S., ... Riese, M. (2014). Interaction of gravity waves with the QBO: A satellite perspective. *Journal of Geophysical Research: Atmospheres*, *119*, 2329 - 2355. doi: https://doi.org/10.1002/2013JD020731

Espinosa, Z. I., Sheshadri, A., Cain, G. R., Gerber, E. P., & DallaSanta, K. J. (2022). Machine learning gravity wave parameterization generalizes to capture the qbo and response to increased co2. *Geophysical Research Letters*, *49*(8), e2022GL098174. doi: https://doi.org/10.1029/2022GL098174

Fovell, R., Durran, D., & Holton, J. (1992). Numerical simulations of convectively generated stratospheric gravity waves. *Journal of Atmospheric Sciences*, *49*(16), 1427–1442.

Fritts, D. C., & Alexander, M. (2003). Gravity wave dynamics and effects in the middle atmosphere. *Reviews of geophysics*, *41*(1).

Geller, M. A., Alexander, M. J., Love, P. T., Bacmeister, J., Ern, M., Hertzog, A., ... Zhou, T. (2013a). A comparison between gravity wave momentum fluxes in observations and climate models. *J. Atmos. Sci.*, *26*(17).

Geller, M. A., Alexander, M. J., Love, P. T., Bacmeister, J., Ern, M., Hertzog, A., ... others (2013b). A comparison between gravity wave momentum fluxes in observations and climate models. *Journal of Climate*, *26*(17), 6383–6405.

Giorgetta, M. A., Sawyer, W., Lapillonne, X., Adamidis, P., Alexeev, D., Clément, V., ... Stevens, B. (2022). The icon-a model for direct qbo simulations on gpus (version icon-cscs:baf28a514). *Geoscientific Model Development*, *15*(18), 6985–7016. doi: 10.5194/gmd-15-6985-2022

Gupta, A., Reichert, R., Dörnbrack, A., Garny, H., Eichinger, R., Polichtchouk, I., ... Birner, T. (2024). Estimates of southern hemispheric gravity wave momentum fluxes across observations, reanalyses, and kilometer-scale numerical weather prediction model. *Journal of the Atmospheric Sciences*, *81*(3), 583–604.

Gupta, A., Sheshadri, A., & Anantharaj. (2024). Gravity wave momentum fluxes from 1 km global ecmwf integrated forecast system. *Scientific Data*, *11*(903). doi: 10.1038/s41597-024-03699-x

Haase, J. S., Alexander, M. J., Hertzog, A., Kalnajs, L. E., Deshler, T., Davis, S. M., ... Venel, S. (2018). Around the world in 84 days [Dataset]. *Eos*, *99*. doi: https://doi.org/10.1029/2018EO091907

Hertzog, A. (2007). The stratéole-vorcore long-duration balloon experiment: A personal perspective. *Space Research Today*, *169*, 43-48. doi: https://doi.org/10.1016/S1752-9298(07)80047-8

Hines, C. O. (1997). Doppler-spread parameterization of gravity-wave momentum deposition in the middle atmosphere. part 2: Broad and quasi monochromatic spectra, and implementation. *J. Atmos. Solar Terr. Phys.*, *59*(4), 387-400. doi: 10.1016/S1364-6826(96)00080-6

Hohenegger, C., Korn, P., Linardakis, L., Redler, R., Schnur, R., Adamidis, P., ... others (2023). Icon-sapphire: simulating the components of the earth system and their interactions at kilometer and subkilometer scales. *Geoscientific Model Development*, *16*(2), 779–811.

Jewtoukoff, V., Plougonven, R., & Hertzog, A. (2013). Gravity waves generated by deep tropical convection: Estimates from balloon observations and mesoscale simulations. *Journal of Geophysical Research: Atmospheres*, *118*(17), 9690-9707. doi: https://doi.org/10.1002/jgrd.50781

Koldunov, N., Kölling, T., Pedruzo-Bagazgoitia, X., Rackow, T., Redler, R., Sidorenko, D., ... Ziemen, F. A. (2023). *nextgems: output of the model development cycle 3 simulations for icon and ifs.* World Data Center for Climate (WDCC) at DKRZ. doi: 10.26050/WDCC/nextGEMS_cyc3

Kruse, C. G., Alexander, M. J., Hoffmann, L., van Niekerk, A., Polichtchouk, I., Bacmeister, J. T., ... others (2022). Observed and modeled mountain waves from the surface to the mesosphere near the drake passage. *Journal of the Atmospheric Sciences*, *79*(4), 909–932.

Köhler, L., Green, B., & Stephan, C. C. (2023). Comparing loon superpressure balloon observations of gravity waves in the tropics with global storm-resolving models. *Journal of Geophysical Research: Atmospheres*, *128*(15), e2023JD038549. doi: https://doi.org/10.1029/2023JD038549

Lilly, D., & Kennedy, P. (1973). Observations of a stationary mountain wave and its associated momentum flux and energy dissipation. *Journal of Atmospheric Sciences*, *30*(6), 1135–1152.

Lindborg, E. (2015). A helmholtz decomposition of structure functions and spectra calculated from aircraft data. *Journal of Fluid Mechanics*, *762*, R4. doi: 10.1017/jfm.2014.685

Lott, F. (1999). Alleviation of stationary biases in a GCM through a mountain drag parameterization scheme and a simple representation of mountain lift forces. *Monthly Weather Review*, *127*(5), 788 - 801. doi: 10.1175/1520-0493(1999)127⟨0788:AOSBIA⟩2.0.CO;2

Lott, F., & Guez, L. (2013a). A stochastic parameterization of the gravity waves due to convection and its impact on the equatorial stratosphere. *J. Geophys. Res.*, *118*(16), 8897-8909. doi: 10.1002/jgrd.50705

Lott, F., & Guez, L. (2013b). A stochastic parameterization of the gravity waves due to convection and its impact on the equatorial stratosphere. *Journal of Geophysical Research: Atmospheres*, *118*(16), 8897–8909.

Lott, F., Guez, L., & Maury, P. (2012). A stochastic parameterization of non-orographic gravity waves: Formalism and impact on the equatorial stratosphere. *Geophys. Res. Lett.*, *39*(6), L06807. doi: 10.1029/2012GL051001

Lott, F., & Miller, M. J. (1997). A new subgrid-scale orographic drag parametrization: Its formulation and testing. *Quarterly Journal of the Royal Meteorological Society*, *123*(537), 101–127.

Lott, F., Rani, R., Podglajen, A., Codron, F., Guez, L., Hertzog, A., & Plougonven, R. (2023). Direct comparison between a non-orographic gravity wave drag scheme and constant level balloons. *Journal of Geophysical Research: Atmospheres*, *128*(4), e2022JD037585.

Matsuoka, D., Watanabe, S., Sato, K., Kawazoe, S., Yu, W., & Easterbrook, S. (2020). Application of deep learning to estimate atmospheric gravity wave parameters in reanalysis data sets. *Geophysical Research Letters*, *47*(19), e2020GL089436. doi: https://doi.org/10.1029/2020GL089436

McLandress, C., & Shepherd, T. G. (2009). Simulated anthropogenic changes in the brewer–dobson circulation, including its extension to high latitudes. *Journal of Climate*, *22*(6), 1516–1540.

Orr, A., Bechtold, P., Scinocca, J., Ern, M., & Janiskova, M. (2010). Improved middle atmosphere climate and forecasts in the ecmwf model through a nonorographic gravity wave drag parameterization. *Journal of Climate*, *23*(22), 5905 - 5926. doi: https://doi.org/10.1175/2010JCLI3490.1

Palmer, T. N., Shutts, G. J., & Swinbank, R. (1986). Alleviation of a systematic westerly bias in general circulation and numerical weather prediction models through an orographic gravity wave drag parametrization. *Quarterly Journal of the Royal Meteorological Society*, *112*(474), 1001-1039. doi: 10.1002/qj.49711247406

Plougonven, R., & Zhang, F. (2014). Internal gravity waves from atmospheric jets and fronts. *Reviews of Geophysics*, *52*(1), 33–76.

Polichtchouk, I., Van Niekerk, A., & Wedi, N. (2023). Resolved gravity waves in the extratropical stratosphere: Effect of horizontal resolution increase from o (10) to o (1) km. *Journal of the Atmospheric Sciences*, *80*(2), 473–486.

Procházková, Z., Kruse, C. G., Alexander, M. J., Hoffmann, L., Bacmeister, J. T., Holt, L., ... Šácha, P. (2023). Sensitivity of mountain wave drag estimates on separation methods and proposed improvements. *Journal of the Atmospheric Sciences*, *80*(7), 1661 - 1680. doi: 10.1175/JAS-D-22-0151.1

Rabier, F., Bouchard, A., Brun, E., Doerenbecher, A., Guedj, S., Guidard, V., ... Steinle, P. (2010, January). The Concordiasi Project in Antarctica. *Bulletin of the American Meteorological Society*, *91*(1), 69-86. doi: 10.1175/2009BAMS2764.1

Richter, J. H., Sassi, F., & Garcia, R. R. (2010). Toward a physically based gravity wave source parameterization in a general circulation model. *Journal of the Atmospheric Sciences*, *67*(1), 136 - 156. doi: 10.1175/2009JAS3112.1

Scinocca, J. F. (2003). An accurate spectral nonorographic gravity wave drag parameterization for general circulation models. *Journal of the Atmospheric Sciences*, *60*(4), 667 - 682. doi: https://doi.org/10.1175/1520-0469(2003)060⟨0667:AASNGW⟩2.0.CO;2

Scinocca, J. F., & McFarlane, N. A. (2000). The parametrization of drag induced by stratified flow over anisotropic orography. *Quarterly Journal of the Royal Meteorological Society*, *126*(568), 2353-2393. doi: https://doi.org/10.1002/qj.49712656802

Serva, F., Cagnazzo, C., Riccio, A., & Manzini, E. (2018). Impact of a stochastic nonorographic gravity wave parameterization on the stratospheric dynamics of a general circulation model. *Journal of Advances in Modeling Earth Systems*, *10*(9), 2147-2162. doi: https://doi.org/10.1029/2018MS001297

Smith, R. B., & Kruse, C. G. (2018). A gravity wave drag matrix for complex terrain. *Journal of the Atmospheric Sciences*, *75*(8), 2599 - 2613. doi: 10.1175/JAS-D-17-0380.1

Song, I.-S., & Chun, H.-Y. (2005). Momentum flux spectrum of convectively forced internal gravity waves and its application to gravity wave drag parameterization. part i: Theory. *J. Atmos. Sci.*, *62*(1), 107-124. doi: https://doi.org/10.1175/JAS-3363.1

Stephan, C. C., Duras, J., Harris, L., Klocke, D., Putman, W. M., Taylor, M., ... Ziemen, F. (2022). Atmospheric energy spectra in global kilometre-scale models. *Tellus A: Dynamic Meteorology and Oceanography*(74(1)), 280-299. doi: 10.16993/tellusa.26

Stephan, C. C., Strube, C., Klocke, D., Ern, M., Hoffmann, L., Preusse, P., & Schmidt, H. (2019). Gravity waves in global high-resolution simulations with explicit and parameterized convection. *Journal of Geophysical Research: Atmospheres*, *124*(8), 4446–4459.

Stevens, B., Satoh, M., Auger, L., Biercamp, J., Bretherton, C. S., Chen, X., ... Zhou, L. (2019). Dyamond: the dynamics of the atmospheric general circulation modeled on non-hydrostatic domains. *Progress in Earth and Planetary Science*, *6*(61). doi: 10.1186/s40645-019-0304-z

Sun, Y. Q., Hassanzadeh, P., Alexander, M. J., & Kruse, C. G. (2023). Quantifying 3d gravity wave drag in a library of tropical convection-permitting simulations for data-driven parameterizations. *Journal of Advances in Modeling Earth Systems*, *15*(5), e2022MS003585.

Tandeo, P., Pulido, M., & Lott, F. (2015). Offline parameter estimation using enkf and maximum likelihood error covariance estimates: Application to a subgrid-scale orography parametrization. *Quarterly Journal of the Royal Meteorological Society*, *141*(687), 383-395. doi: https://doi.org/10.1002/qj.2357

Toghraei, I. (2024). *imantoghraei/parameterization_icon: Icon.* Zenodo. Retrieved from `https://doi.org/10.5281/zenodo.13946360` ([Collection])

Voelker, G. S., Bölöni, G., Kim, Y.-H., Zängl, G., & Achatz, U. (2024). Ms-gwam: A three-dimensional transient gravity wave parametrization for atmospheric models. *Journal of the Atmospheric Sciences*, *81*(7), 1181 - 1200. doi:

10.1175/JAS-D-23-0153.1

Warner, C. D., & McIntyre, M. E. (1999). Toward an ultra-simple spectral gravity wave parameterization for general circulation models. *Earth, Planets and Space*, *51*, 475–484. doi: 10.1186/BF03353209

Wedi, N. P., Polichtchouk, I., Dueben, P., Anantharaj, V. G., Bauer, P., Boussetta, S., . . . Vitart, F. (2020). A baseline for global weather and climate simulations at 1 km resolution. *Journal of Advances in Modeling Earth Systems*, *12*(11), e2020MS002192. doi: https://doi.org/10.1029/2020MS002192

Wei, J., Zhang, F., Richter, J. H., Alexander, M., & Sun, Y. Q. (2022). Global distributions of tropospheric and stratospheric gravity wave momentum fluxes resolved by the 9-km ecmwf experiments. *Journal of the Atmospheric Sciences*, *79*(10), 2621–2644.

Supporting Information for "Can parameterizations reproduce the gravity waves momentum fluxes and drag simulated by a global high-resolution model?"

I. Toghraei[1], F. Lott[1], L. Köhler[2], C. C. Stephan[3], M. J. Alexander[4]

[1]Laboratoire de Météorologie Dynamique, Institut Pierre-Simon Laplace, PSL Research Institute, Paris, France.

[2]Alfred Wegener Institute, Bremerhaven, Germany.

[3]Leibniz Institute of Atmospheric Physics, University of Rostock, Kühlungsborn, Germany.

[4]NorthWest Research Associates, Boulder Office, Boulder, CO, USA

Contents of this file

Introduction

This supporting information provides two additional figures to the main article. Figure S1 shows the global distribution of the "sign definite" positive and negative zonal momentum fluxes resolved by ICON and predicted by the parameterization schemes. Figure S2 compares vertical profiles of east and west momentum fluxes resolved by ICON and predicted by the parameterization schemes.

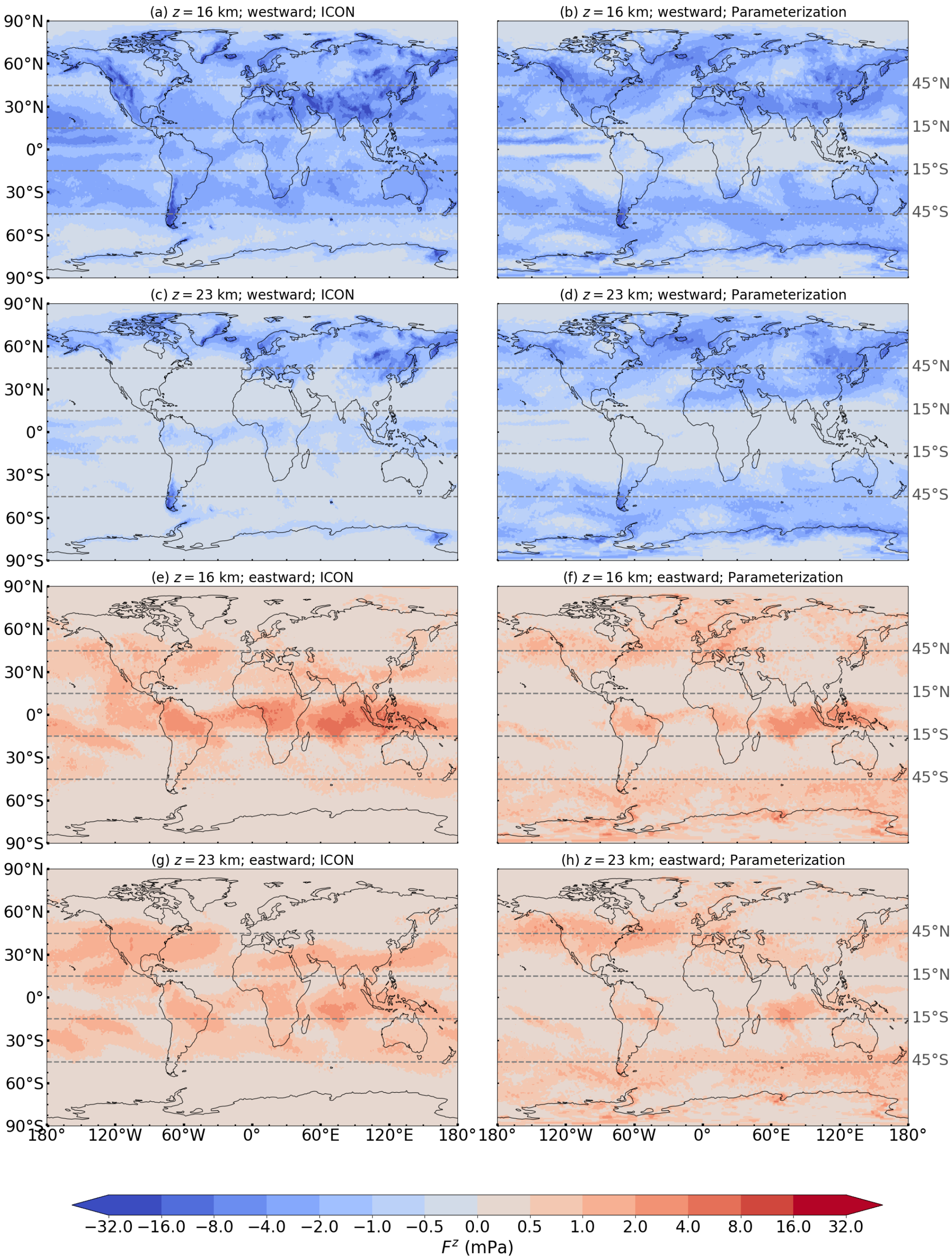

Figure S1. Global distribution of the 21-day mean of the "sign definite" positive (eastward) and negative (westward) zonal momentum fluxes resolved by ICON (left) and predicted by the parameterization schemes (right). The eastward fluxes are in the top four panels, the westward ones in the bottom four panels. The altitude is $z = 16$ km in (a,b,e,f) and $z = 23$ km in (c,d,g,h).

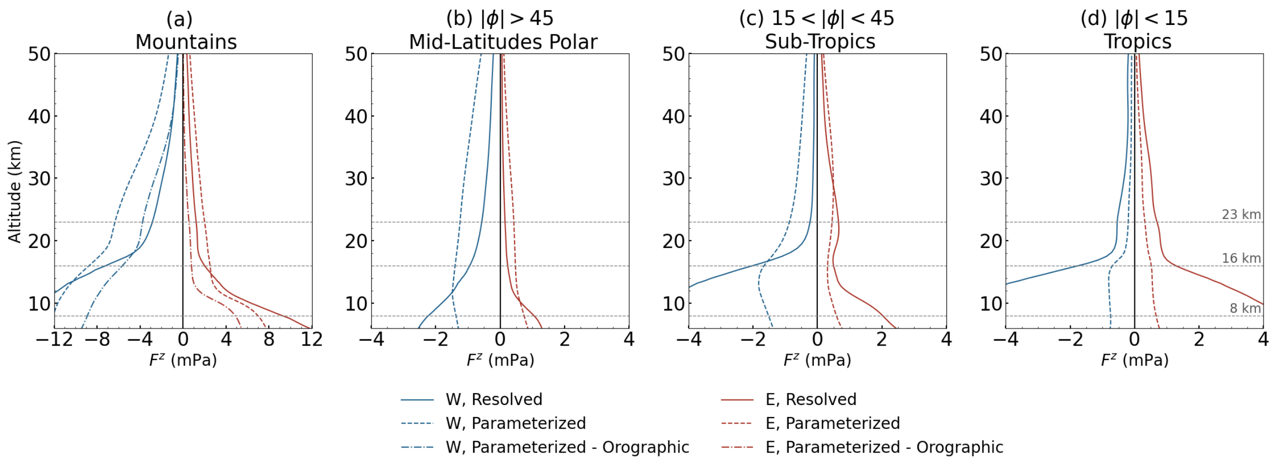

Figure S2. Vertical profile of the ”sign definite” eastward (red) and westward (blue) zonal momentum fluxes resolved by ICON (solid lines) and predicted by the parameterization schemes (dashed lines) in 4 different sectors we have used so far to characterize the momentum flux behaviour, i.e. mountainous regions, defined as standard deviation of subgrid-scale orography $\sqrt{[h'^2]} > 100$ m, and non-mountainous regions (land and ocean) in the mid-latitudes ($|\phi| > 45^o$), the subtropics ($15^o < |\phi| < 45^o$), and the tropics ($|\phi| < 15^o$).Over mountain regions, the fluxes from the orographic GW parameterization scheme are shown with a dashed-dotted line.